New light on the Kr(4p55s2) Feshbach resonances: high-resolution electron scattering experiments and B-spline R-matrix calculations

T H Hoffmann, M.-W Ruf, H Hotop, O Zatsarinny, K Bartschat, M Allan

New light on the $Kr^-(4p^5 5s^2)$ Feshbach resonances: high resolution electron scattering experiments and B-spline R-matrix calculations

T. H. Hoffmann[1,2], M.-W. Ruf[1], H. Hotop[1], O. Zatsarinny[3], K. Bartschat[3] and M. Allan[2]

[1] *Fachbereich Physik, Technische Universität KL, 67653 Kaiserslautern, Germany*

[2] *Department of Chemistry, University of Fribourg, 1700 Fribourg, Switzerland*

[3] *Department of Physics and Astronomy, Drake University, Des Moines, Iowa 50311, USA*

(Dated: February 11, 2010; submitted to J. Phys. B)

In a joint experimental and theoretical effort, we carried out a detailed study of electron scattering from Kr atoms in the energy range of the low-lying $Kr^-(4p^5 5s^2)$ Feshbach resonances. Absolute angle-differential cross sections for elastic electron scattering were measured over the energy range 9.3−10.3 eV with an energy width of about 13 meV at scattering angles between 10° and 180°. Using several sets of elastic scattering phase shifts, a detailed analysis of the sharp Kr^- $(4p^5 5s^2\,{}^2P_{3/2})$ resonance was carried out, resulting in a resonance width of $\Gamma_{3/2} = 3.6(2)$ meV. By direct comparison with the position of the Ar^- $(3p^5 4s^2\,{}^2P_{3/2})$ resonance, the energy for the Kr^- $(4p^5 5s^2\,{}^2P_{3/2})$ resonance was determined as $E_{3/2} = 9.489(3)$ eV. A Fano-type fit of the higher-lying Kr^- $(4p^5 5s^2\,{}^2P_{1/2})$ resonance yielded the resonance parameters $\Gamma_{1/2}$= 33(5) meV and $E_{1/2} = 10.126(4)$ eV. In order to obtain additional insight, *B*-spline *R*-matrix calculations were performed for both the elastic and the inelastic cross sections above the threshold for $4p^5$ 5s excitation. They provide the total and angle differential cross sections for excitation of long-lived and short lived levels of the $4p^5$ 5s configuration in Kr and branching ratios for the decay of the Kr^- $(4p^5 5s^2\,{}^2P_{1/2})$ resonance into the three available exit channels. The results are compared with selected experimental data.

I. INTRODUCTION

The lowest Feshbach resonances of the rare gases are among the sharpest features known in electron scattering. They may be considered as two spin-paired Rydberg electrons surrounding a relatively compact positive core. A review of their properties can be found in the article by Schulz [1], which was later updated by Buckman and Clark [2]. In recent experiments with energy widths as small as 4 meV, the lowest Feshbach resonances of He [3, 4], Ne [5], and Ar [4] were studied in unprecedented detail, and more accurate resonance widths and energies than previously available were determined. These resonances can only decay to the respective ground states and

have very small widths (He^- ($1s2s^2\,^2S_{1/2}$): 10.9(3) meV [3, 4], Ne^- ($2p^53s^2\,^2P_{3/2,1/2}$): 1.27(7) meV [5], Ar^- ($3p^54s^2\,^2P_{3/2,1/2}$): 2.3(2) meV[4]). For Kr, on the other hand, the fine-structure splitting between the two Kr^- ($4p^55s^2\,^2P_{3/2,1/2}$) resonances is much larger than in Ne and Ar, such that the higher-lying Kr^- ($4p^55s^2\,^2P_{1/2}$) resonance can decay to three exit channels, namely to the ground state Kr ($4p^6\,^1S_0$) and, in addition, to the two excited Kr ($4p^55s\,^3P_{2,1}$) levels plus a free electron (threshold energies 9.915 eV and 10.032 eV, respectively). Correspondingly, the width of the Kr^- ($4p^55s^2\,^2P_{1/2}$) resonance is much larger (about 30 meV [6]). It is of obvious interest to characterize the size and the resonance shapes in the partial cross sections for the three exit channels.

The Kr^- ($4p^55s^2\,^2P_{3/2,1/2}$) resonances were first observed (but not characterized) by Schulz [7]. Kuyatt *et al.* [8] and Sanche and Schulz [9] measured them in improved transmission experiments. Angle-differential cross sections at 45° were reported by Swanson *et al.* [10]. From an analysis of resonance profiles measured at several angles, Weingartshofer *et al.* [11] deduced a width for the Kr^- ($4p^55s^2\,^2P_{3/2}$) resonance of 8 meV. Heindorff *et al.* [12] observed the resonance at 115° and investigated the angular distribution over the energy range 3.0−10.5 eV. In conjunction with measurements of the excitation of long-lived Kr levels, Brunt *et al.* [13] gave the energy positions of the resonances as 9.484 eV and 10.123 eV, respectively. Using threshold electron spectroscopy, Jureta *et al.* [14] obtained the value 10.119(5) eV for the position of the Kr^- ($4p^55s^2\,^2P_{1/2}$) resonance. From a consistent analysis of the Kr^- ($4p^55s^2\,^2P_{3/2}$) resonance profile measured at 19 angles, Dubé *et al.* [15] deduced a natural width of 3.6(4) meV. Zubek *et al.* [6] observed the resonances at angles up to 180° with a magnetic angle changer [16, 17], extracting widths of $\Gamma_{3/2} = 3.5(10)$ meV and $\Gamma_{1/2} = 30(4)$ meV, respectively.

In the present paper, we report the results of a joint experimental and theoretical study of electron scattering from Kr atoms in the energy range of the low-lying $Kr^-(4p^55s^2)$ Feshbach resonances with the aim to shed new light on the dynamics of the addressed processes. Two different experimental setups were used to study elastic electron scattering from Kr atoms in the energy range from 9.3 eV to 10.3 eV with improved energy resolution (13 meV).

This paper is organized as follows: In section II we briefly describe the two experiments carried out in Kaiserslautern and Fribourg. Section III sketches the analysis of the resonance profiles and outlines the *B*-spline *R*-matrix (BSR) method used in the present numerical calculations. In section IV we present the experimental results and their analyses and compare them with previous measurements and the BSR predictions. Moreover, computed angle-differential cross sections for near-threshold excitation of the four levels of the $Kr(4p^55s)$ configuration will be compared with

experimental results of Phillips [18]. We conclude with a brief summary.

II. EXPERIMENT

A. Experiment at Kaiserslautern

The electron scattering setup involving a laser photoelectron source was described in detail previously [3–5]. Briefly, potassium atoms from an atomic beam source are excited by a Ti:Sa laser to the $K^*\,(4p\,^2P_{3/2})$ level that is ionized at threshold with a focused blue intracavity dye laser. The photolectrons are extracted by a weak electric field (≈ 10 V/m) and imaged onto the atomic target beam. Five retarding-field electron detectors at fixed angles count the elastically scattered electrons. The triply differentially pumped supersonic target beam nearly eliminates Doppler broadening [3, 5]. For Kr, problems associated with cluster formation occur at the usual nozzle temperature of 300 K (see also [4]). To reduce clustering, the nozzle was heated up to 470 K. Unfortunately, the heating reduced the energy resolution (energy width around 10 meV) as a result of quickly varying surface potentials, presumably due to fluctuations in the potassium coverage of the surfaces. As a consequence, the photoelectron apparatus was mainly used for an energy calibration of the $Kr^-\,(4p^5 5s^2\,^2P_{3/2})$ resonance.

B. Experiment at Fribourg

Electrons emitted from a hot filament are energy-selected by a double hemispherical monochromator and focused onto an effusive beam target, introduced by a 0.25 mm nozzle kept at about 30°C. A double hemispherical analyzer for detection of elastically or inelastically scattered electrons ensures background-free signals [19]. Absolute cross sections are determined by comparison against He using a relative-flow method [20]. A specially designed magnetic angle changer allows for measurements up to 180° scattering angle [21]. For the present measurements of elastic scattering at energies around 10 eV, the angular acceptance amounts to 3° full width at half maximum (FWHM); the uncertainty of the angular position is estimated as ±1°. Procedures for ensuring reliable cross sections were described in detail elsewhere [22, 23]. The confidence limit (two standard deviations) for the absolute cross sections is about ±15%. The incident electron resolution was about 13 meV at a beam current of about 400 pA.

III. THEORY

A. Phase-shift analysis of resonance scattering profiles

Elastic scattering of electrons from a heavy rare gas atom can be treated as potential scattering in the presence of spin-orbit coupling. The differential cross section $\mathrm{d}\sigma(\theta)/\mathrm{d}\Omega$ then depends upon both the direct scattering amplitude $f(E,\theta)$ and the spin-flip amplitude $g(E,\theta)$ [24] according to

$$\frac{\mathrm{d}\sigma}{\mathrm{d}\Omega}(E,\theta) = |f(E,\theta)|^2 + |g(E,\theta)|^2. \tag{1}$$

These amplitudes can be written as partial-wave sums

$$f(E,\theta) = \frac{1}{2ik}\sum_{l=0}^{\infty}\left[(l+1)\left(e^{2i\delta_l^+}-1\right) + l\left(e^{2i\delta_l^-}-1\right)\right]P_l(\cos\theta) \tag{2}$$

and

$$g(E,\theta) = \frac{1}{2ik}\sum_{l=1}^{\infty}\left(e^{2i\delta_l^+} - e^{2i\delta_l^-}\right)P_l^1(\cos\theta), \tag{3}$$

where the wave vector of the electron is given by $k = \sqrt{2mE}/\hbar$ while $P_l(\cos\theta)$ and $P_l^1(\cos\theta)$ $(l \geq 1)$ denote the standard and associated Legendre polynomials, respectively. For partial waves with orbital angular momentum $l \geq 1$, the total angular momenta $J^+ = l + 1/2$ and $J^- = l - 1/2$ experience different phase shifts δ_l^+ and δ_l^-. The influence of the resonances can be described by additional phase shifts

$$\delta_{res}^{\pm} = -\mathrm{arccot}\,\frac{2(E - E_{res}^{\pm})}{\Gamma_{\pm}} \tag{4}$$

that change by π over an interval given by the natural width $\Gamma_{\pm}$. For higher partial waves $l > l_c$ (with typical values of $l_c \approx 3$), the interaction is dominated by the long-range polarization potential. An expression due to Thompson [25],

$$f_{l>l_c} = \frac{\pi\alpha k}{a_0}\left(\frac{1}{3} - \frac{1}{2}\sin\frac{\theta}{2} - \sum_{l=1}^{l_c}\frac{P_l(\cos\theta)}{(2l-1)(2l+3)}\right) \tag{5}$$

with α denoting the static dipole polarizability $(2.4844(12) \times 10^{-30}\ \mathrm{m}^3$ [26]) allows for calculating their influence.

B. BSR calculations

The present calculations were performed with the semi-relativistic (Breit-Pauli) B-spline R-matrix (BSR) (close-coupling) program of Zatsarinny [27], as well as a recently developed fully

relativistic version [28]. An important feature of this code is the ability to define non-orthogonal sets of one-electron orbitals, which generally allow for a highly accurate target description with relatively small (compared to standard approaches with orthogonal orbitals) configuration-interaction expansions. Below we will present results from a semi-relativistic 47-state model (BSR47), which was already successfully applied to studying the excitation of metastable levels in Kr [29], and from a fully relativistic model with 32 states. Of the latter, 31 are physical states (the same as the lowest 31 states of the BSR47 model) plus a pseudo-state that was constructed to ensure the correct dipole polarizability of the ground state. This model will be denoted as DBSR31p below.

1. The BSR47 model

The target description used for Kr is based on the same philosophy as those described in detail for Ne [30] and Ar [31]. We started by generating the $1s - 4p$ core orbitals from a Hartree-Fock calculation for Kr^+. Important correlation effects, which should be included in the calculation of the excited states of Kr, are the significant core-valence correlation and the strong term-dependence of the valence orbitals. There is also very strong configuration mixing between the $4p^4(n+1)s$ and $4p^4nd$ states and, finally, one may want to account for inner-core correlation effects.

In the present approach, we treat the core-valence correlation *ab initio* by adding target configurations with an excited core. Standard multi-configuration expansions, however, can become very large and are hardly employable in subsequent scattering calculations. For this reason, we used the B-spline box-based close-coupling method described by Zatsarinny and Froese Fischer [32] to generate the target states.

Only the $(4s^2 4p^5\ ^2P_{3/2,1/2})$ states were used as target states in the B-spline bound-state expansion. In order to account for the core-valence correlation, the close-coupling expansion for the target states also included configurations with an excited core, $4p^4\overline{5}\ell\overline{5}\ell'$, where the $\overline{5}\ell$ ($\ell = 0, 1, 2, 3$) correlation orbitals were optimized in separate multi-configuration Hartree-Fock calculations for each term. In order to limit the bound-state expansions to an acceptable size, we only kept configurations with expansion coefficients greater than 0.01. The above procedure allowed us to reduce the error in the binding energies for the lowest $4p^5 5s$ and $4p^5 4d$ states from 0.35 eV to 0.13 eV, indicating that we indeed included a substantial amount of core-valence correlation.

Core correlation effects were included by single and double promotion of the 4s and 4p orbitals to $\overline{4}\ell$ correlation orbitals, but we only kept configurations with expansion coefficients larger than 0.025. The main contributions come from the $4s4p^5\overline{4}d$, $4s^2 4p^3\overline{4}d^2$, and $4s^2 4p^4\overline{4}f$ configurations. These are

considered sufficient to include the most important inner-core correlation effects with a minimum number of correlation configurations.

The number of physical states that we can generate by this method depends on the radius a of the R-matrix box. Our choice of $a = 50\ a_0$, where $a_0 = 0.529 \times 10^{-10}$ m denotes the Bohr radius, yields a good description for the 31 spectroscopic states with dominant configurations $4p^5 5s$, $4p^5 5p$, $4p^5 4d$ and $4p^5 6s$, respectively. The 16 additional states with dominant configurations $4p^5[J=3/2]5d, 6p, 7s$ are also described fairly well, but one would generally not expect coupling to these target states to be very important for the energy range considered for this work. Instead, coupling to the ionization continuum may be important (see below), but performing such calculations with a large number of pseudo-states goes beyond our currently available computational resources.

We emphasize that the above procedure generates *non-orthogonal*, *term-dependent* sets of radial functions for each individual state, also accounting for term mixing due to the spin-orbit interaction. In the present calculations, the atomic Hamiltonian includes all one-electron Breit-Pauli operators plus the two-electron spin-other-orbit interaction. The relativistic corrections are very important in Kr, which is already too heavy to expect excellent *ab initio* results in a perturbative approach with non-relativistic orbitals. Consequently, in order to reproduce the correct term mixing we used the experimental value of $\zeta(4p) = 0.666\,\mathrm{eV}$ as the spin-orbit parameter for the 4p orbital. In contrast, the non-relativistic wavefunction for the $4s^2 4p^5$ core yields $\zeta(4p) = 0.602\,\mathrm{eV}$, thus requiring a 10% adjustment.

2. The DBSR31p model

Here we started by generating the core orbitals (spinors) from a Kr^+ Dirac-Fock calculation using the `GRASP2K` relativistic atomic-structure package [33]. Next, the valence 5s and 4d orbitals in the $4p^4 5s$ and $4p^4 4d$ configurations were generated in a frozen-core calculation for Kr^+ in the average-term approximation. All these states of Kr^+ were then used as target states in B-spline bound-state close-coupling calculations to generate the low-lying states of atomic Kr. The corresponding close-coupling expansion had the structure

$$\begin{aligned}\Phi(5p^5 nl, J\pi) \;&=\; \mathcal{A}\sum_i \left\{\varphi(4p^5)\phi(n_i l_i)\right\}^{J\pi} \\ &+\; \mathcal{A}\sum_i \left\{\varphi(4p^4 5s)\phi(n_i l_i)\right\}^{J\pi}\end{aligned}$$

$$
\begin{aligned}
&+ \ \mathcal{A}\sum_i \left\{\varphi(4\mathrm{p}^4 4\mathrm{d})\phi(n_i l_i)\right\}^{J\pi} \\
&+ \ \mathcal{A}\sum_i \left\{\varphi(4\mathrm{s}4\mathrm{p}^6)\phi(n_i l_i)\right\}^{J\pi} \\
&+ \ a\varphi(4\mathrm{p}^6) \qquad (6)
\end{aligned}
$$

where $\mathcal{A}$ denotes the anti-symmetrization operator. The unknown large and small radial components for the outer valence electron, $\phi(n\ell)$, were expanded in individual B-spline bases. The coefficients of these expansions were found by diagonalizing the Dirac-Coulomb hamiltonian with the additional requirement that the wavefunctions vanish at the boundary. Note that we require orthogonality of the physical $\phi(n\ell)$ orbitals only to the core orbitals $1\mathrm{s} - 4\mathrm{p}$, but not to the 5s and 4d orbitals of Kr^+ that are considered here as correlation orbitals. More details of this procedure can be found in [28].

The first sum in Eqn. (6) represents the physical valence states under consideration, while the next three sums were included to describe the core-valence correlation. Although the above close-coupling expansion can also generate the $4\mathrm{p}^6$ ground state, we explicitly added the initial one-configuration wavefunction of this state for a more extended description of the relaxation effects in the 4s and 4p orbitals for this case. As mentioned above, for an accurate calculation of term mixing in Kr it is crucial to use the correct value of the spin-orbit parameter for the 4p orbital. In contrast to the Breit-Pauli approach, the Dirac-Coulomb method yields $\zeta(4\mathrm{p}) = 0.665\,\mathrm{eV}$. This is very close to the experimental value of 0.666 eV, and hence we do not need an adjustment in this case. Consequently, the present structure model is indeed fully *ab initio*.

The above scheme again yields non-orthogonal, term-dependent orbitals $\phi(n\ell)$ for each Kr state. However, the present Dirac-Coulomb approach differs from our Breit-Pauli calculations for noble-gas atoms regarding the description of the core-valence correlation. Instead of employing specially designed correlation orbitals (see previous subsection) for this purpose, using the box-based close-coupling ansatz directly to account for the various terms and the interaction between them in the jj-coupling scheme resulted in 37 core states in the expansion (6). This scheme yields a relatively small (up to 120 terms) configuration-interaction expansions for the final target states of Kr. On the other hand, it produced a very large number of different non-orthogonal orbitals (about 3,000), which were then employed in the description of all target states. As in BSR47, the size of the R-matrix box was chosen as $a = 50\,a_0$, and we obtained a good description of the physical states with $n \leq 6$.

In contrast to previous work, however, we then constructed one more odd-parity pseudo-state

with total electronic angular angular momentum $J = 1$. This state was designed to ensure that its coupling to the ground state produced the correct dipole polarizability. Since most of the dipole polarizability of the noble-gas ground states originates from coupling to the continuum, this is the simplest and widely used method of accounting for this effect in a coupled-channel calculation. [In single-channel calculations, a popular alternative method is to add a polarization term to the scattering potential.]

The present method reproduced the binding energies with an accuracy of better than 80 meV for all states in neutral Kr. We consider this highly accurate, given the complete *ab initio* character of these calculations and the relatively small size of the configuration expansions. In the subsequent scattering calculations, however, we used the experimental excitation energies. This allowed us to compare directly with experiment, especially regarding the near-threshold resonance structure. It is worth noting that our procedure of adjusting the target energies effectively corresponds to small stretches or contractions of the energy scale between the various thresholds [27]. Since we do not force orthogonality between the target and the projectile orbitals (see next subsection), we do not have to include $(N + 1)$-electron "bound-bound" terms in the close-coupling expansion of the collision problem. As a result, using the experimental thresholds does not carry the danger of otherwise possible inconsistencies in the relative positions of the N-electron target and the $(N + 1)$-electron resonance states.

Before we describe the collision calculations, it is important to note that the structure models described above are not quite as sophisticated as those generated in the structure-only mode of the BSR and DBSR codes [34]. This is due to the fact that the projectile electron has to be coupled in as well, and hence a compromise has to be made in the number of target configurations that can be included in a practical collision calculation. Nevertheless, the accuracy did not deteriorate substantially, and we believe that the current target descriptions are an adequate basis for the scattering calculations. Also, while they should describe very similar physics (except for the additional pseudo-state in the DBSR31p model), the details of the calculations, including the codes used, are very different. Hence, they provide a valuable cross-check between the two approaches and the associated computer programs.

3. Collision Calculations

We used the published BSR code [27] and our newly developed DBSR version [28] to solve the $(N+1)$-electron collision problem. The essential idea is to expand the basis of continuum orbitals

used to describe the projectile electron inside the R-matrix box, i.e., the region where the problem is most complicated due to the highly correlated motion of $N+1$ electrons, also in terms of a B-spline basis. A semi-exponential grid for the B-spline knot sequence was set up to cover the inner region up to the R-matrix radius. We used the same grid for the structure and the collision calculations. For $a = 50\,a_0$, we employed 82 splines in the Breit-Pauli model and 111 in the Dirac approach for the Kr target. The latter increase was necessary to correctly describe the finite-size nuclear model with a Fermi potential adopted in the present work.

Note that the DBSR calculations lead to significantly larger interaction matrices in the internal region compared to the BSR calculations, due to the additional treatment of the small spinor components. In the DBSR31p calculations, which included up to 124 scattering channels, interaction matrices with dimensions of about 25,000 needed to be diagonalized. In order to perform those calculations we had to parallelize the DBSR code and also used parallelized linear-algebra libraries such as `SCALAPACK`.

We calculated partial-wave contributions up to $J = 51/2$ numerically. No extrapolation scheme to account for even higher partial waves was necessary for all observables presented in this paper. The cross sections of interest were then calculated in the same way as in the standard R-matrix approach. We employed an updated version [35] of the flexible asymptotic R-matrix (`FARM`) package by Burke and Noble [36] to solve the problem in the asymptotic region and to obtain the transition matrix elements of interest. After transforming the latter from the present jj-coupling to the jlK-coupling scheme and also accounting for the appropriate phase convention of the reduced matrix elements, we employed the program `MJK` of Grum-Grzhimailo [37] to calculate the angle-differential cross sections shown below.

IV. EXPERIMENTAL RESULTS AND DISCUSSION

A. Nonresonant elastic scattering

The differential cross sections for elastic electron scattering from Kr, measured at an energy of 9.8 eV, are compared with selected calculated DCS in figure 1. The full circles with error bars indicate the experimental absolute measurements at several discrete angles, the open circles result from magnetic scans with 1° increment, recorded at three fixed detector positions (45°, 90°, 135°) and normalized as described in [4, 22]. The largest (relative) deviations occur at angles around the minimum near 117°, where the experimental data are best reproduced when the phase shifts of

Sauter and Meyer [45] and Fon *et al.* [42] are used. The optical potential calculations of McEachran and Stauffer [46] at 10 eV (not shown in the figure) yield the minimum at 118°, but their minimum DCS (obtained from figure 1 of [46]) is almost a factor of 2 higher than our measured value.

At forward and backward angles, deviations of up to 20% are observed between the various data sets. The BSR47 results for angles up to 30° suffer from the fact that coupling to just discrete states only accounts for 30% of the dipole polarizability of the ground state. As mentioned above, this problem can be fixed by adding specially constructed pseudo-states to the R-matrix (close-coupling) expansion, as done by Fon *et al.* [42] and Bell *et al.* [43] who concentrated on elastic scattering, and also in our DBSR31p model as described above. Clearly, including for the polarization of the ground state in the DBSR31p model considerably improves the agreement with experiment.

The absolute values of our DCS are listed in table I, which also contains the results of four previous measurements at an energy of 10 eV [38–41]. A graphical comparison between the earlier results can be found in [38]. According to BSR calculations carried out at 9.8 eV and 10.0 eV, the DCS at small and large angles vary little with energy (<3%) while the DCS at the minimum increases by 18% towards higher energy. Except in the angular range around the minimum of the DCS, good to excellent agreement is found between our data and those of Cho *et al.* [39] and Linert *et al.* [38]. At small angles, our DCS agree best with those of Danjo [40], whose values become progressively too large at angles above 70°. The data of Srivastava *et al.* [41] are 10% to 30% smaller than our results at angles below 110°, and 15% to 87% larger at higher angles.

The influence of the finite angular resolution on the measured depth of the minimum DCS is such that the apparent cross section in the minimum is raised by 13%, 29%, and 51% when the theoretical DCS, calculated by the DBSR31p method, is convoluted with a Gaussian angular resolution profile of 4°, 6°, and 8° FWHM, respectively. Since all experiments were carried out with an angular acceptance width lower than ±3° (FWHM < 6°), the observed differences in the apparent cross section close to the minimum are too large to be accounted for solely by angular resolution effects. The deeper minimum of our data may be due to the especially low background of the Fribourg apparatus.

B. Characterization of the Kr^- ($4p^5 5s^2\ ^2P_{3/2,1/2}$) resonances

The Kr^- ($4p^5 5s^2\ ^2P_{3/2}$) resonance below the excitation threshold is much sharper and more prominent than the higher-lying Kr^- ($4p^5 5s^2\ ^2P_{1/2}$) resonance that can decay into three exit chan-

nels. The properties of the Kr^- ($4p^5 5s^2\,{}^2P_{3/2}$) resonance, which is only coupled to the elastic scattering channel, can be accurately determined through a standard partial-wave analysis, once reliable phase shifts are known. New energy-dependent spectra of this resonance, measured in Fribourg at seven different angles, are shown in figure 2 as open circles. The absolute scale is fixed with reference to the experimental angular distribution. The measured data were fitted by a resonance profile calculated from a few sets of phase shifts (see table II) and adjustable values of the resonance width $\Gamma_{3/2}$ and of the experimental energy width ΔE (full width half maximum of a Gaussian function) common to all angles. Small deviations between the experimental and the calculated non-resonant cross sections were compensated by angle-dependent correction factors. For the fits in figure 2, these factors differed from unity by less than 7%. The optimal values $\Gamma_{3/2}$ and ΔE thus obtained are summarized in table III.

The quality of the fit was judged by the sum of the squared residuals (SSR); the numerical quality factor Q of a fit was obtained by dividing the minimal SSR through the SSR resulting from a given set of phase shifts. Thus, a Q of 1.0 was assigned to the fit based on the phase shifts of Sauter and Meyer [45], which yielded the best agreement. The phase shifts by Fon *et al.* [42] resulted in a higher, those by Bell *et al.* [43] and Sienkiewicz and Baylis [44] in a smaller width. The weighted mean of the different fits results in a value of 3.58(20) meV for the width of the Kr^- ($4p^5 5s^2\,{}^2P_{3/2}$) resonance. Using the phase shifts of Sauter and Meyer [45], fits at individual angles were carried out for comparison; for each angle, we give the natural width Γ and experimental energy width ΔE (Angle: Γ (meV) / ΔE (meV)): 10°: 3.62 / 12.1; 22.5°: 3.68 / 11.6; 45°: 3.64/12.1; 90°: 3.40/11.6; 112.5°: 2.62/12.0; 135°: 3.71/11.9; 180°: 3.77/13.6. Since the angular distributions for Kr and Ar in the vicinity of the resonance positions are similar, the very small natural width at 112.5° comes as no surprise. It shows the influence of remaining uncertainties in the differential cross section around the minimum, as already discussed for Ar by Franz *et al.* [4].

Our experimental value for the width of the Kr^- ($4p^5 5s^2\,{}^2P_{3/2}$) resonance is compared with previous results in table IV. Excellent agreement with the values of Dubé *et al.* [15] and Zubek *et al.* [6] is observed. The widths of 2.9 meV obtained in the DBSR31p model and the even smaller value of 2.7 meV from the BSR47 calculation show consistency between two very independent calculations, but these widths appear to be too small. Unfortunately, it looks as if the apparent improvement achieved in the BSR47 model in the target description and the angle-integrated metastable excitation function [29] does not carry over to the details of the Kr^- ($4p^5 5s^2\,{}^2P_{3/2,1/2}$) resonances.

The position of the Kr^- ($4p^5 5s^2\,{}^2P_{3/2}$) resonance was determined relative to that of the

Ar^- ($3p^5 4s^2\,{}^2P_{3/2}$) resonance in the photoelectron setup using a mixed supersonic Ar-Kr beam. From a fit to the measured line profiles, we obtain a resonance energy of 9.489(3) eV. Within the mutual uncertainties, this value agrees with the results of Brunt *et al.* [13], Jureta *et al.* [14] and Zubek *et al.* [6] (see table V).

In figure 3, we present the measured energy dependence of the DCS over a broader energy range (9.3−10.3 eV), encompassing the higher-lying Kr^- ($4p^5 5s^2\,{}^2P_{1/2}$) resonance as well. As mentioned previously, the latter can also decay into the two nearby excited levels Kr ($4p^5 5s\,{}^3P_{2,1}$). Since this decay is almost ten times more rapid than that to the ground state, it leads to a total width of 33(5) meV. This width is the average value, as determined from fits to the profiles measured at the angles 10°, 22.5°, 45°, 135° and 180°. For these fits, Shore profiles [47, 48] were used and convoluted with a Gaussian function to account for the experimental resolution of about 13 meV. The observed angular variation of the line profiles for both resonances is in good agreement with that reported by Weingartshofer *et al.* [11] at an energy width of 30 meV. Once again the BSR47 model gives a significantly smaller total width for this resonance (15.4 meV) than the DBSR31p calculation (31.9 meV), with the latter being in better agreement with experiment. The large difference in the widths predicted by the BSR47 and DBSR31p models indicates a strong sensitivity of the results on the details of the model. This makes a theoretical description very challenging.

In figure 4, results of the DBSR31p and BSR47 calculations for the angular dependence of the resonance profiles are presented and compared with the lineshapes derived from the fits to the experimental data. Note that all profiles are shown *without* convolution with the Gaussian resolution function. The variation of the experimentally deduced lineshapes with angle is well recovered by the BSR calculations with a preference for the BSR47 results while the DBSR31p results yield resonance widths closer to the experimental values (see Table IV).

C. Differential cross sections for electron-impact excitation of Krypton to the $4p^5 5s$ levels

In a forthcoming paper [29], BSR calculations of the total cross sections for excitation of the metastable Kr ($4p^5 5s\,{}^3P_{2,0}$) and of the VUV-emitting Kr ($4p^5 5s\,{}^3P_1, {}^1P_1$) levels are reported and found to be in good agreement with experimental data of the Manchester group [13, 51, 52]. A more sensitive test of the BSR description for electron scattering from Kr is provided by angle-differential cross sections for inelastic processes near threshold. Phillips [18] reported such measurements for excitation of the four levels in the Kr($4p^5\,5s$) configuration at three angles (30°, 55°, 90°) from threshold up to about 14 eV. Her absolute cross sections, measured with an energy width of 35 meV,

were extracted in digitized form from the respective figures in [18] and are shown in figures 5, 6, and 7.

Comparison with the results from both the DBSR31p and BSR47 calculations shows encouraging qualitative agreement with respect to the position and energy dependence of the principal features up to incident energies of about 12.5 eV. The models do not contain a sufficient number of states to expect such agreement for higher energies. Both the experimental and the calculated angle-differential cross sections in figures 5-7 (and also the angle-integrated cross section [29, 51]) for formation of the VUV emitting Kr $(4p^5 5s\,^3P_1)$ level demonstrate a strong enhancement of this inelastic channel through the decay from the Kr^- $(4p^5 5s^2\,^2P_{1/2})$ resonance. In contrast, production of the Kr $(4p^5 5s\,^3P_2)$ level via this resonance is much less pronounced. This different behavior is explained by the fact that the $^2P_{1/2}$ resonance can decay to the barrier-free $Kr(^3P_1)+e^-$ $(l = 0)$ s-wave channel, but not to the $Kr(^3P_2)+e^-(l = 0)$ channel. In agreement with these considerations, the DBSR31p (BSR47) calculations predict angle-integrated relative partial widths of about 8%, 6%, and 86% (20%, 9%, 71%) for the decay of the $^2P_{1/2}$ resonance to the ground and the Kr $(4p^5 5s\,^3P_2)$ and Kr $(4p^5 5s\,^3P_1)$ states, respectively. These partial widths were calculated with the time-delay method of Smith [53] for obtaining the decay probabilities of a given resonance into different final channels.

Below the $Kr(^3P_1)$ threshold, at about 10.01 eV, another sharp resonance feature shows up in the calculated DCS for the inelastic $Kr(^3P_2)$ channel, which is expected to be due to a (shape) resonance with the configuration $4p^5(^2P_{3/2})5s5p(^3P)$ [2]. In the review of Buckman and Clark, the position of the lowest resonance with the configuration $4p^5(^2P_{3/2})5s5p(^3P)$ is given as 10.039(10) eV; this value was derived from the appearance of a peak labeled "b" in the metastable Kr excitation function just above the $Kr(^3P_2)$ threshold.

There are clearly problems with the magnitude of the cross-section values, particularly at a scattering angle of 55°. These problems could be related to the angular dependence of the cross sections, i.e., a comparison at the nominal scattering without accounting for the angular resolution in the experiment may be misleading. Further work will need to be done to analyze the remaining discrepancies.

V. CONCLUSIONS

The Kr^- $(4p^5 5s^2\,^2P_{3/2,1/2})$ resonances in elastic electron scattering from Kr atoms were measured at an improved energy resolution (13 meV). For the Kr^- $(4p^5 5s^2\,^2P_{3/2})$ resonance, a nat-

ural width of 3.6(2) meV was deduced from a partial-wave analysis of the angle-dependent resonance profiles. The resonance energy was determined as 9.489(3) eV with reference to the position of the sharp Ar^- ($3p^5 4s^2\,{}^2P_{3/2}$) Feshbach resonance (11.103(1) eV [4, 50]). The higher-lying Kr^- ($4p^5 5s^2\,{}^2P_{1/2}$) resonance (position 10.126(4) eV) was analyzed by Fano-type fits to the measured profiles, resulting in a width of 33(5) meV. This much larger value results from the strong decay of this resonance to the excited Kr ($4p^5 5s\,{}^3P_1$) level. Both the DBSR31p and the BSR47 calculations predict that the $^2P_{1/2}$ resonance decays predominantly to the nearby Kr ($4p^5 5s\,{}^3P_1$) + e^- channel.

The variation of the experimental lineshapes with angle is well recovered by the BSR calculations. However, the width of the Kr^- ($4p^5 5s^2\,{}^2P_{3/2}$) resonance is predicted about 20%−25% smaller than our experimental result of 3.6 ± 0.2 meV, which is in good agreement with previous measurements. Regarding the Kr^- ($4p^5 5s^2\,{}^2P_{1/2}$) resonance, the fully relativistic DBSR31p model, which accounts for long-range polarization effects, predicts a width of ≈ 32 meV, in good agreement with experiment (33 ± 5 meV). On the other hand, the BSR47 model (a slightly different structure description, more coupled states, but without accounting for polarization effects due to coupling to the target continuum) predicts a much smaller width of only ≈ 15 meV for this resonance.

Unfortunately, it is currently not possible for us to pin down a single reason for the remaining discrepancies between experiment and theory in the resonance widths and the apparently high sensitivity of the theoretical results for the width of the Kr^- ($4p^5 5s^2\,{}^2P_{1/2}$) resonance. We suspect it to be a combination of the background description and the fact that the latter resonance position is so close to threshold that any small difference in the predicted position will also affect the calculated width very strongly. This becomes even more important due to the fact that the theoretical excitation thresholds need to be adjusted to reproduce the experimental energy splittings and thus to allow for a direct comparison between experiment and theory. While these adjustments are very small in the present case and the BSR approach due to the lack of $(N+1)$-electron terms in the close-coupling expansion is generally much less sensitive to this adjustment procedure than the standard Belfast R-matrix approach, we cannot rule out that it is at least partially responsible for the sensitivity seen in our results. These findings, as well as the comparison with the angle- and final-state-resolved cross sections of Phillips [18], emphasize the need for further high-resolution precision experiments as well as continued theoretical efforts to fully understand the intricacies of these collision processes.

401 **Acknowledgments**

402 This work was supported by the Deutsche Forschungsgemeinschaft (grant HO427/28), by the
403 "Forschungszentrum Optische Technologien und Lasergesteuerte Prozesse", by the European Sci-
404 ence Foundation through the network EIPAM ("Electron-Induced Processing At the Molecular
405 level" Exchange Grant No. 1288), by the Swiss National Science Foundation (project No. 200020-
406 121841), and the United States National Science Foundation under grants #PHY-0757755 and
407 #PHY-0903818, as well as the Teragrid allocation MCA08X034. We thank K. Franz for exper-
408 imental support in the early phase of the project. We gratefully acknowledge W. Meyer and
409 G. Sauter for providing their scattering phase shifts for Kr and M. Zubek for sending a preprint of
410 ref. [38].

---

411 [1] G. J. Schulz, Rev. Mod. Phys. **45**, 378 (1973).
412 [2] S. J. Buckman and C. W. Clark, Rev. Mod. Phys. **66**, 539 (1994).
413 [3] A. Gopalan, J. Bömmels, S. Götte, A. Landwehr, K. Franz, M. W. Ruf, H. Hotop, and K. Bartschat,
414 Eur. Phys. J. D **22**, 17 (2003).
415 [4] K. Franz, T. H. Hoffmann, J. Bömmels, A. Gopalan, G. Sauter, W. Meyer, M. Allan, M.-W. Ruf, and
416 H. Hotop, Phys. Rev. A **78**, 012712 (2008).
417 [5] J. Bömmels, K. Franz, T. H. Hoffmann, A. Gopalan, O. Zatsarinny, K. Bartschat, M.-W. Ruf, and
418 H. Hotop, Phys. Rev. A **71**, 012704 (2005).
419 [6] M. Zubek, B. Mielewska, J. Channing, G. C. King, and F. H. Read, J. Phys. B: At. Mol. Opt. Phys.
420 **32**, 1351 (1999).
421 [7] G. J. Schulz, Phys. Rev. **136**, A650 (1964).
422 [8] C. E. Kuyatt, J. A. Simpson, and S. R. Mielczarek, Phys. Rev. **138**, A385 (1965).
423 [9] L. Sanche and G. J. Schulz, Phys. Rev. A **5**, 1672 (1972).
424 [10] N. Swanson, J. W. Cooper, and C. E. Kuyatt, Phys. Rev. A **8**, 1825 (1973).
425 [11] A. Weingartshofer, K. Willmann, and E. M. Clarke, J. Phys. B: At. Mol. Phys. **7**, 79 (1974).
426 [12] T. Heindorff, J. Hofft, and P. Dabkiewicz, J. Phys. B: At. Mol. Phys. **9**, 89 (1976).
427 [13] J. N. H. Brunt, G. C. King, and F. H. Read, J. Phys. B: At. Mol. Phys. **9**, 2195 (1976).
428 [14] J. Jureta, S. Cvejanovic, J. N. H. Brunt, and F. H. Read, J. Phys. B: At. Mol. Phys. **11**, L347 (1978).
429 [15] D. Dubé, D. Tremblay, and D. Roy, Phys. Rev. A **47**, 2893 (1993).
430 [16] F. H. Read and J. M. Channing, Rev. Sci. Instrum. **67**, 2372 (1996).
431 [17] M. Zubek, N. Gulley, G. C. King, and F. H. Read, J. Phys. B: At. Mol. Opt. Phys. **29**, L239 (1996).
432 [18] J. M. Phillips, J. Phys. B: At. Mol. Phys. **15**, 4259 (1982).

433 [19] M. Allan, J. Phys. B: At. Mol. Opt. Phys. **25**, 1559 (1992).

434 [20] J. C. Nickel, P. W. Zetner, G. Shen, and S. Trajmar, J. Phys. E: Sci. Instrum. **22**, 730 (1989).

435 [21] M. Allan, J. Phys. B: At. Mol. Opt. Phys. **33**, L215 (2000).

436 [22] M. Allan, J. Phys. B: At. Mol. Opt. Phys. **38**, 3655 (2005).

437 [23] M. Allan, J. Phys. B: At. Mol. Opt. Phys. **40**, 3531 (2007).

438 [24] N. F. Mott and H. S. W. Massey, *The theory of atomic collisions* (Oxford University Press, Oxford,
439 1965), 3rd ed.

440 [25] D. G. Thompson, Proc. Roy. Soc. A, Math. and Phys. Sci. **294**, 160 (1966).

441 [26] D. R. Lide, ed., *T. M. Miller in CRC Handbook of Chemistry and Physics* (CRC Press (Taylor &
442 Francis), Boca Raton, 2008), 88th ed.

443 [27] O. Zatsarinny, Comp. Phys. Commun. **174**, 273 (2006).

444 [28] O. Zatsarinny and K. Bartschat, Phys. Rev. A **77**, 062701 (2008).

445 [29] O. Zatsarinny and K. Bartschat, J. Phys. B: At. Mol. Opt. Phys. **43**, in press (2010).

446 [30] O. Zatsarinny and K. Bartschat, J. Phys. B: At. Mol. Opt. Phys. **37**, 2173 (2004).

447 [31] O. Zatsarinny and K. Bartschat, J. Phys. B: At. Mol. Opt. Phys. **37**, 4693 (2004).

448 [32] O. Zatsarinny and C. F. Fischer, J. Phys. B: At. Mol. Opt. Phys. **35**, 4669 (2002).

449 [33] P. Jönsson, X. He, C. F. Fischer, and I. P. Grant, Comp. Phys. Commun. **177**, 597 (2007).

450 [34] O. Zatsarinny and K. Bartschat, Phys. Scr. **T134**, 014020 (2009).

451 [35] C. J. Noble, private communication (2008).

452 [36] V. M. Burke and C. J. Noble, Comp. Phys. Commun. **85**, 471 (1995).

453 [37] A. N. Grum-Grzhimailo, Comp. Phys. Commun. **152**, 101 (2003).

454 [38] I. Linert, B. Mielewska, G. C. King, and M. Zubek, Phys. Rev. A **81**, 012706 (2010).

455 [39] H. Cho, R. J. Gulley, and S. J. Buckman, J. Kor. Phys. Soc. **42**, 71 (2003).

456 [40] A. Danjo, J. Phys. B: At. Mol. Opt. Phys. **21**, 3759 (1988).

457 [41] S. K. Srivastava, H. Tanaka, A. Chutjian, and S. Trajmar, Phys. Rev. A **23**, 2156 (1981).

458 [42] W. C. Fon, K. A. Berrington, and A. Hibbert, J. Phys. B: At. Mol. Phys. **17**, 3279 (1984).

459 [43] K. L. Bell, K. A. Berrington, and A. Hibbert, J. Phys. B: At. Mol. Opt. Phys. **21**, 4205 (1988).

460 [44] J. E. Sienkiewicz and W. E. Baylis, J. Phys. B: At. Mol. Opt. Phys. **24**, 1739 (1991).

461 [45] G. Sauter and W. Meyer, private communication of preliminary data (2009).

462 [46] R. P. McEachran and A. D. Stauffer, J. Phys. B: At. Mol. Opt. Phys. **36**, 3977 (2003).

463 [47] B. W. Shore, Phys. Rev. **171**, 43 (1968).

464 [48] I. D. Petrov, V. L. Sukhorukov, and H. Hotop, J. Phys. B: At. Mol. Opt. Phys. **41**, 065205 (2008).

465 [49] F. M. J. Pichanick and J. A. Simpson, Phys. Rev. **168**, 64 (1968).

466 [50] P. Hammond, J. Phys. B: At. Mol. Opt. Phys. **29**, L231 (1996).

467 [51] J. N. H. Brunt, G. C. King, and F. H. Read, J. Phys. B: At. Mol. Phys. **10**, 3781 (1977).

468 [52] S. J. Buckman, P. Hammond, G. C. King, and F. H. Read, J. Phys. B: At. Mol. Phys. **16**, 4219 (1983).

469 [53] F. T. Smith, Phys. Rev. **118**, 349 (1960).

TABLE I: Absolute angle-differential cross sections for elastic e–Kr scattering (in 10^{-20}m^2/sr). Comparison of different experimental data measured at 10 eV: Linert *et al.* [38], angular acceptance $\Delta\theta\pm2°$, uncertainty $\pm15\%$; Cho *et al.* [39], $\Delta\theta\pm1.5°$, uncertainty $\pm(7-15)\%$; Danjo [40], $\Delta\theta\pm2°$, uncertainty $\pm20\%$; Srivastava *et al.* [41], $\Delta\theta\pm1.8°$, uncertainty $\pm20\%$; present work (measured at 9.8 eV), $\Delta\theta\pm1.5°$, uncertainty $\pm15\%$.

angle (°)	this work	Linert *et al.*	Cho *et al.*	Danjo	Srivastava *et al.*
10	13.00			13.6	
15	11.02			11.6	
20	9.31		10.637	9.8	7.1
25	7.57		8.659	7.6	5.8
30	6.11	6.246	6.916	6.6	4.6
35	4.88		5.110	5.4	3.8
40	3.84	3.778	3.917	4.4	3.1
45	3.01		2.922	3.2	2.3
50	2.39	2.364	2.400	2.8	1.8
55	1.96		1.928	2.3	1.5
60	1.64	1.568	1.640	1.9	1.3
65	1.45		1.480	1.6	1.2
70	1.33	1.393	1.399	1.6	1.1
75	1.25		1.325	1.8	1.1
80	1.20	1.242	1.220	1.6	1.1
85	1.09		1.112	1.4	1.0
90	0.946	0.907	0.939	1.2	0.84
95	0.783		0.788	1.1	0.68
100	0.559	0.489	0.612	0.79	0.46
105	0.317		0.406	0.54	0.28
110	0.144	0.162	0.218	0.30	0.10
115	0.071	0.136	0.131	0.18	0.084
117	0.063				
120	0.080	0.213	0.142	0.38	0.15
125	0.216		0.278	0.72	0.36
130	0.499	0.613	0.597		0.70
135	0.912		1.344		
140	1.41	1.577	1.781		
145	2.00		2.353		
150	2.64	3.095	2.921		
155	3.30		3.271		
160	3.97	4.377	3.695		
165	4.71		4.098		
170	5.23	4.926	4.325		
175	5.59		4.586		
180	5.72	5.882	4.688		

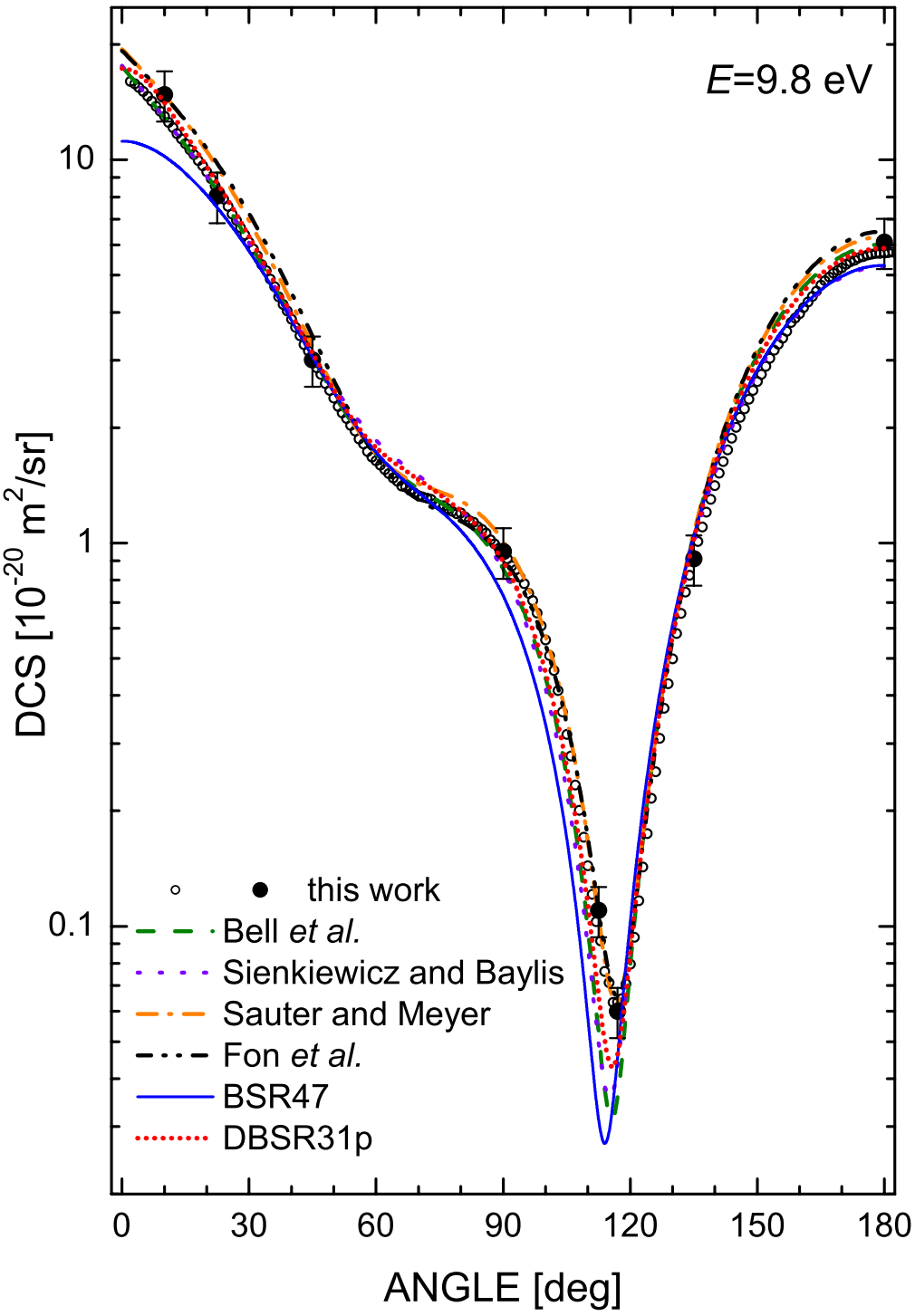

FIG. 1: Differential cross section for elastic e−Kr scattering, measured in Fribourg at an electron energy of 9.8 eV, compared to angular distributions calculated with theoretical phase shifts due to Fon *et al.* [42], Bell *et al.* [43], Sienkiewicz and Baylis [44], and Sauter and Meyer [45]. The full circles with error bars indicate the experimental absolute measurements at several discrete angles, the open circles were obtained from magnetic scans with 1° increment, recorded at three fixed detector positions (45°, 90°, 135°) and normalized as described in [22]. The predictions of the DBSR31p and the BSR47 model are also included. (colour online)

TABLE II: Comparison of phase shifts for elastic e−Kr scattering from different authors (in rad).

Phases from	δ_0(9.5eV)	δ_1(9.5eV)	δ_2(9.5eV)	δ_3(9.5eV)
	δ_0(9.8eV)	δ_1(9.8eV)	δ_2(9.8eV)	δ_3(9.8eV)
Bell *et al.* [43]	-1.260	-0.687	+0.865	+0.132
	-1.283	-0.705	+0.894	+0.137
Fon *et al.* [42]	-1.250	-0.736	+0.955	+0.130
	-1.274	-0.753	+0.986	+0.134
Sienkiewicz and Baylis δ^+ [44]	-1.244	-0.732	+0.825	+0.144
	-1.267	-0.751	+0.854	+0.149
Sienkiewicz and Baylis δ^-		-0.691	+0.828	+0.143
		-0.710	+0.857	+0.148
Sauter and Meyer [45]	-1.182	-0.667	+0.986	+0.155
	-1.206	-0.683	+1.016	+0.162

TABLE III: Width of the Kr^- ($4p^5 5s^2\ ^2P_{3/2}$) resonance when analyzed using different phase shifts (Q: quality factor, see text).

Phases from	Γ (meV)	ΔE (meV)	Q
Bell *et al.* [43]	3.31	12.3	0.32
Fon *et al.* [42]	3.74	12.2	0.52
Sienkiewicz and Baylis [44]	3.30	12.4	0.34
Sauter and Meyer [45]	3.67	12.3	1.00

TABLE IV: Natural width of the Kr^- ($4p^5 5s^2\ ^2P_{3/2,1/2}$) resonances.

	$\Gamma_{3/2}$ (meV)	$\Gamma_{1/2}$ (meV)
Swanson *et al.* [10]	3.8–6.0	
Weingartshofer *et al.* [11]	8	
Dubé *et al.* [15]	3.6(4)	
Zubek *et al.* [6]	3.5(1.0)	30(4)
this work (exp.)	3.6(2)	33(5)
this work (DBSR31p)	2.9	31.9
this work (BSR47)	2.7	15.4

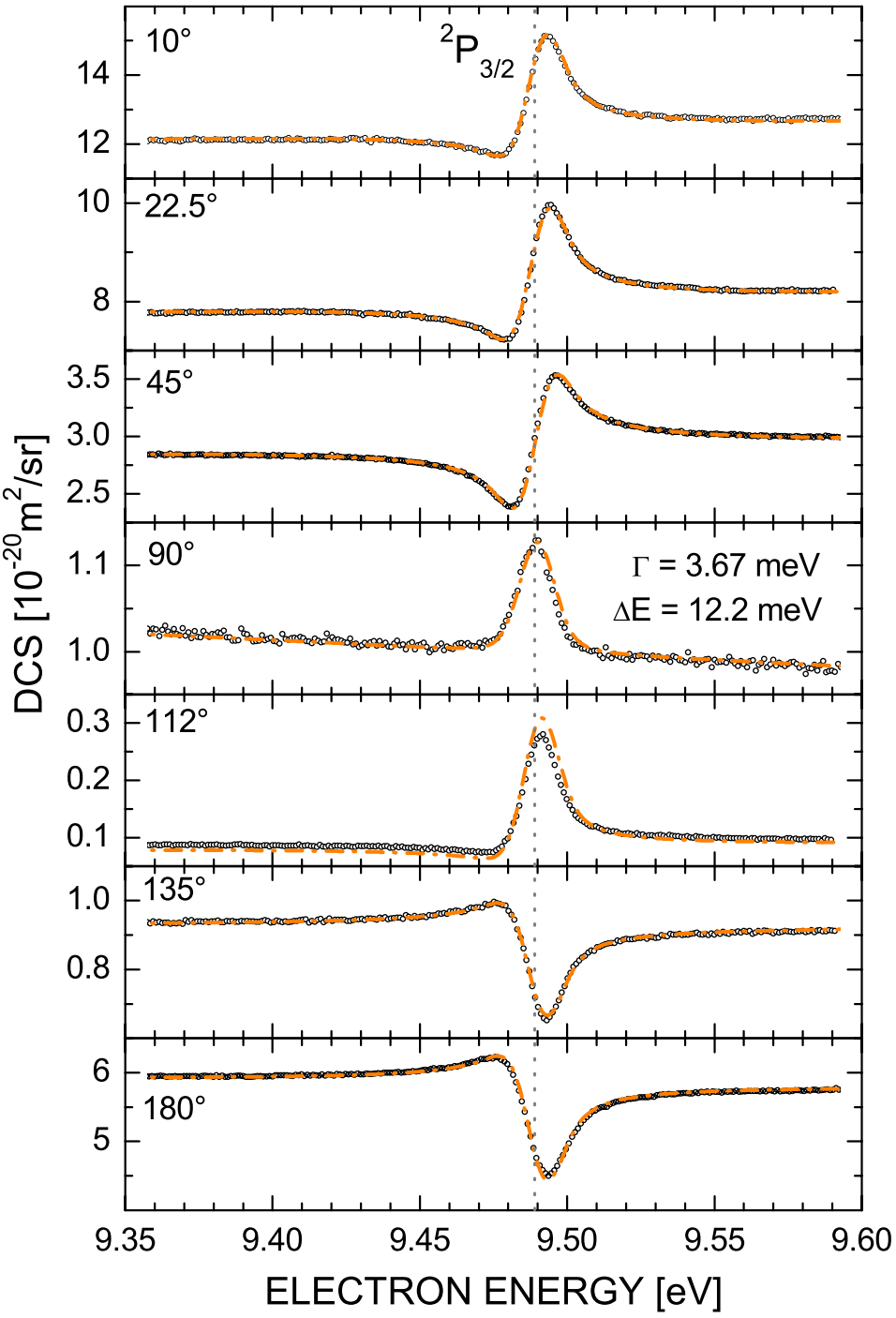

FIG. 2: Differential cross section for elastic e−Kr scattering in the vicinity of the Kr^- ($4p^5 5s^2\,{}^2P_{3/2}$) resonance (open circles: experiment). The line profiles (chain orange curves) were calculated from the phases of Sauter and Meyer [45]. (colour online)

TABLE V: Energy position and fine-structure splitting of the Kr^- ($4p^5 5s^2\ ^2P_{3/2,1/2}$) resonances.

	Energy [eV]		
	$^2P_{3/2}$	$^2P_{1/2}$	Δ_{FS} [meV]
Kuyatt *et al.* [8]	9.45 – 9.48(1)	10.10(1)	640(10)
Pichanick and Simpson [49]		10.05	
Sanche and Schulz [9]	9.50 – 9.53(3)	10.16 – 10.19(3)	660
Swanson *et al.* [10][a]	9.515	10.155	640
Weingartshofer *et al.* [11][b]	9.525(10)	10.162	637(10)
Brunt *et al.* [13]	9.484(10)	10.123	639(3)
Jureta *et al.* [14]	9.490(12)	10.119(5)	
Zubek *et al.* [6][c]	9.485(12)	10.121(15)	636
this work (BSR47)	9.489	10.126	637
this work (BSR31p)	9.488	10.128	640

[a] position of the first resonance by Sanche and Schulz [9] taken as reference

[b] recalibrated values, using 19.365 eV [3] as the energy for the He^- ($1s2s^2\ ^2S_{1/2}$) resonance

[c] relative to the position for the Ar^- ($3p^5 4s^2\ ^2P_{3/2}$) resonance: 11.103 eV [4, 50]

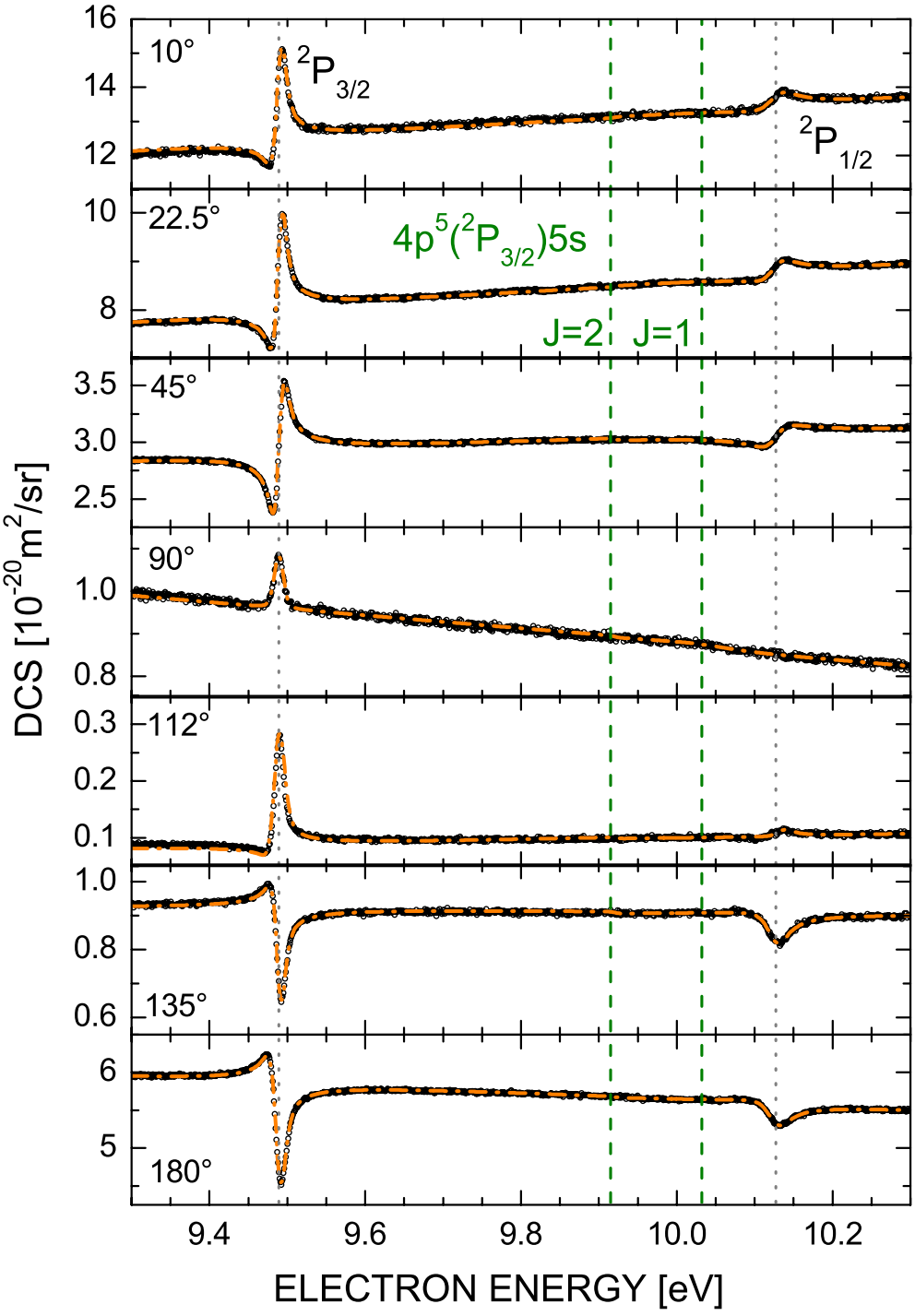

FIG. 3: Differential cross section for elastic e−Kr scattering in the vicinity of the Kr^- ($4p^5 5s^2\,^2P_{3/2,1/2}$) resonances (open circles: experiment). The chain orange curves represent the result of a phase-shift analysis for the Kr^- ($4p^5 5s^2\,^2P_{3/2}$) resonance and Fano-type profiles with appropriate background (see text) for the Kr^- ($4p^5 5s^2\,^2P_{1/2}$) resonance. The broken vertical lines indicate the thresholds for the Kr ($4p^5 5s\,^3P_{2,1}$) levels while the dotted vertical lines represent the positions of the $^2P_{3/2}$ and $^2P_{1/2}$ resonances. (colour online)

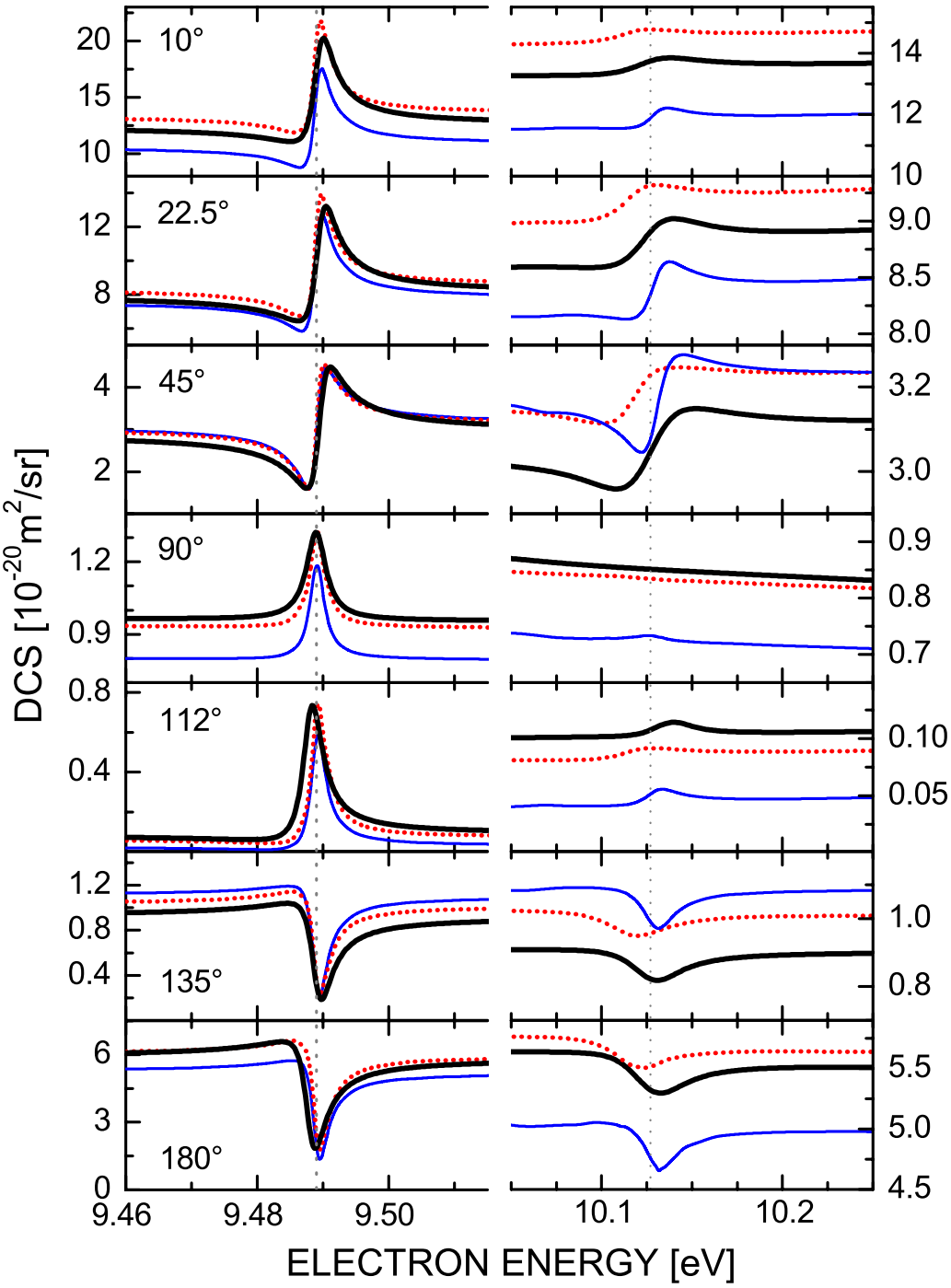

FIG. 4: Differential cross section for elastic e−Kr scattering around the Kr^- ($4p^5 5s^2\,{}^2P_{3/2,1/2}$) resonances. The unconvoluted line shapes, deduced from the fits to the experimental data, are shown as thick black curves and compared with theoretical results obtained from the DBSR31p (dotted red curves) and BSR47 (full blue curves) models (colour online). The dotted vertical lines represent the positions of the $^2P_{3/2}$ and $^2P_{1/2}$ resonances.

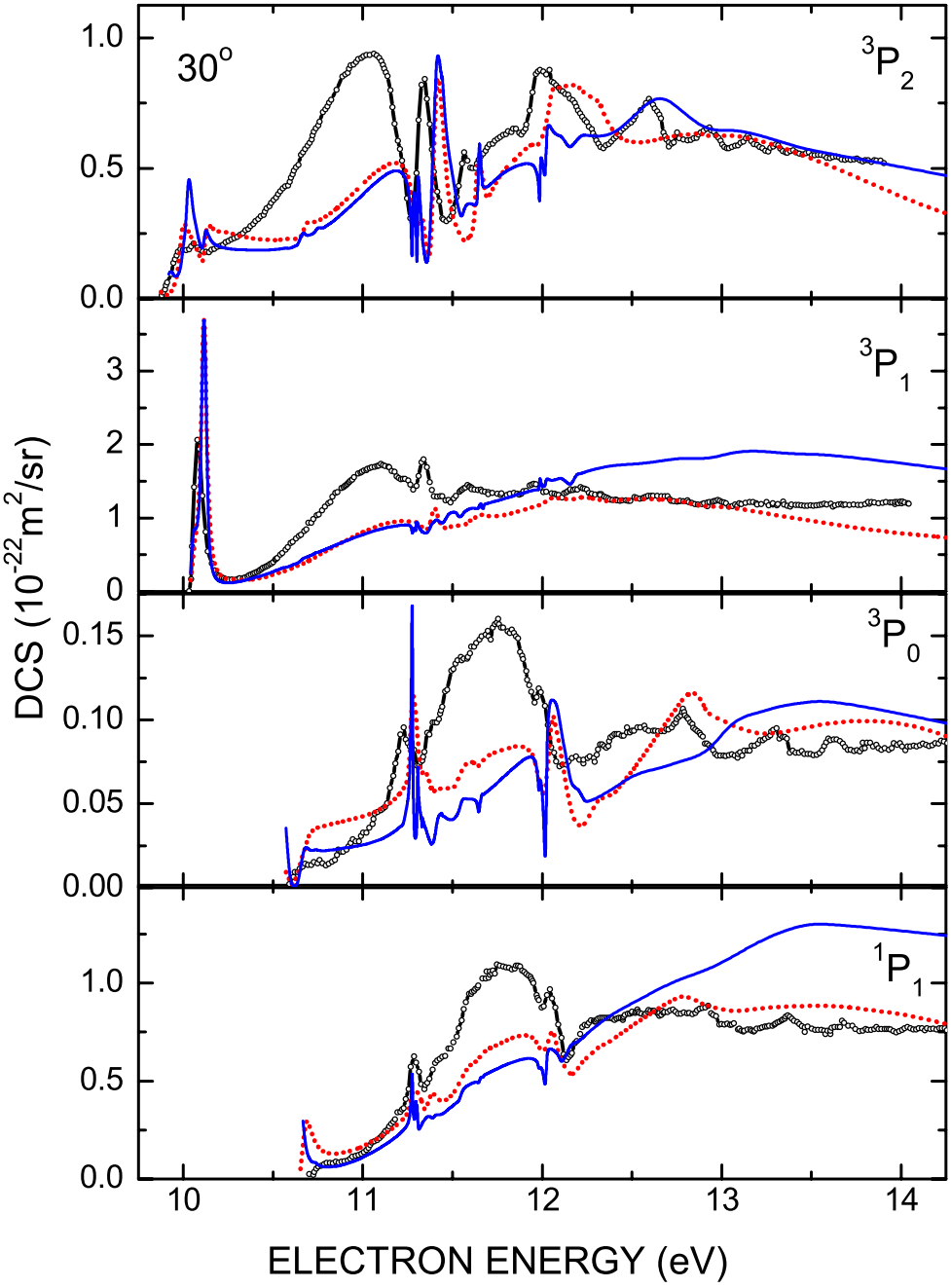

FIG. 5: Differential cross section for electron-impact excitation of Kr at a scattering angle of 30°. The experimental data (open circles; resolution 35 meV) are taken from Phillips by digitizing the data in figure 5 of [18]. They are compared with theoretical results obtained from the DBSR31p (dotted red curves) and BSR47 (full blue curves) models (colour online).

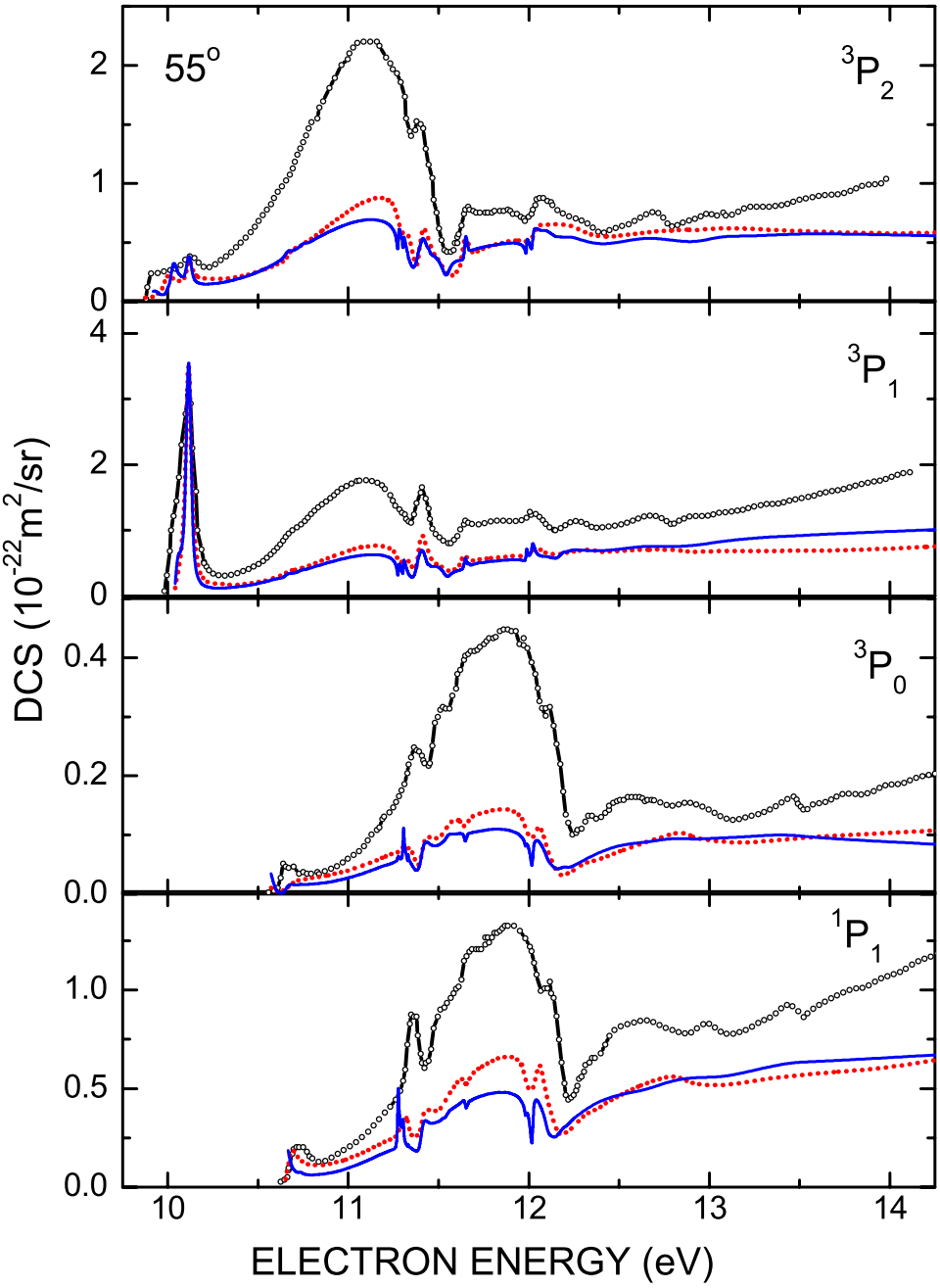

FIG. 6: Differential cross section for electron-impact excitation of Kr at a scattering angle of 55°. The experimental data (open circles; resolution 35 meV) are taken from Phillips by digitizing the data in figure 4 of [18]. They are compared with theoretical results obtained from the DBSR31p (dotted red curves) and BSR47 (full blue curves) models (colour online).

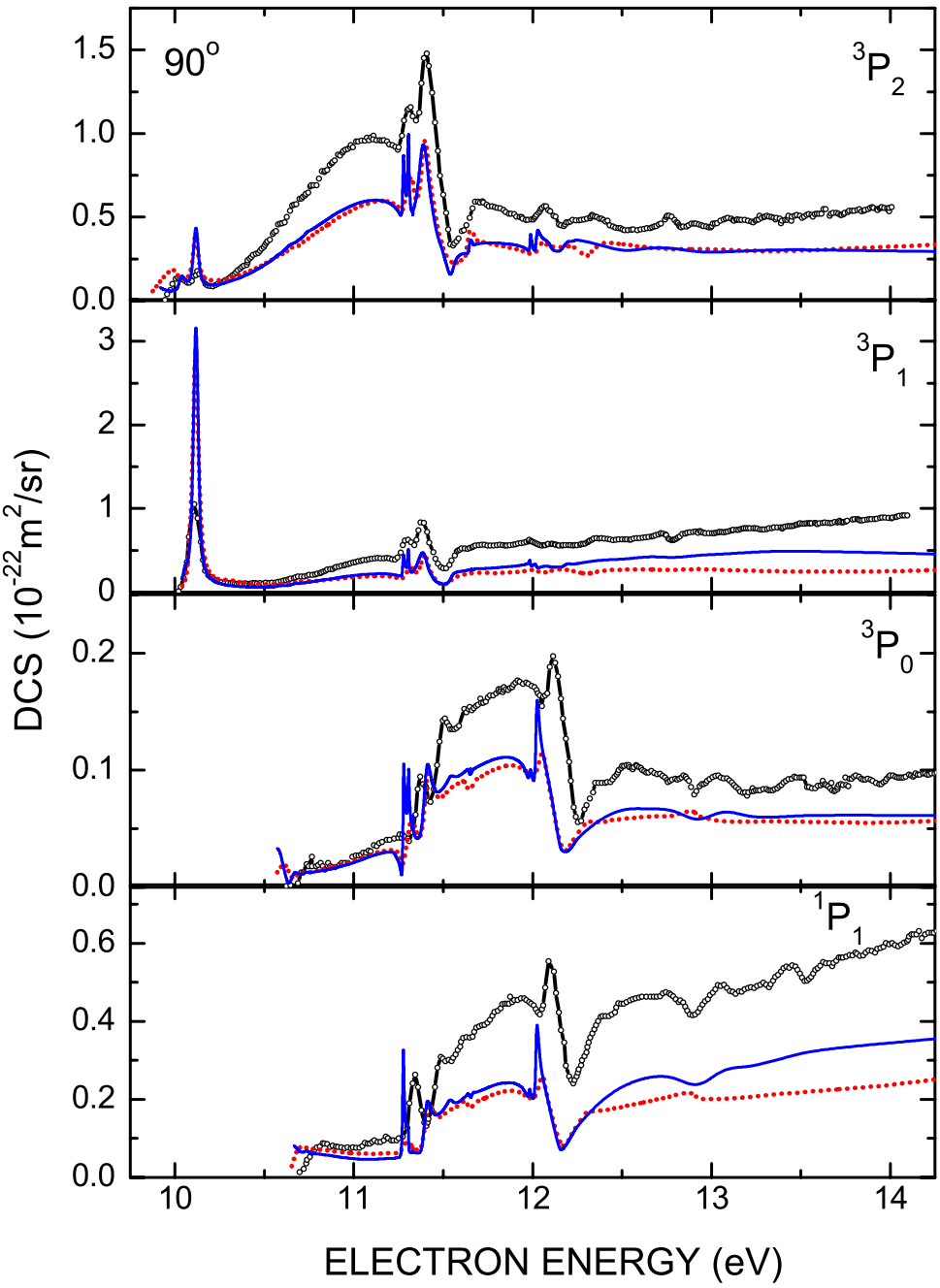

FIG. 7: Differential cross section for electron-impact excitation of Kr at a scattering angle of 90°. The experimental data (open circles; resolution 35 meV) are taken from Phillips by digitizing the data in figure 3 of [18]. They are compared with theoretical results obtained from the DBSR31p (dotted red curves) and BSR47 (full blue curves) models (colour online).